Chem

Homeostatic artificial cells enable self-protection in prototissue spheroids

Graphical abstract

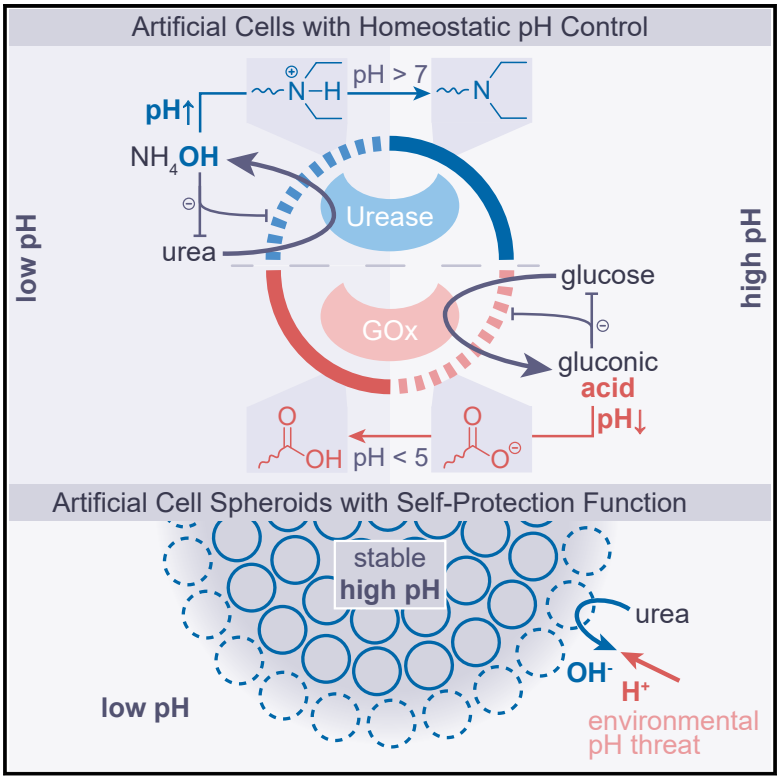

Highlights

- Microfluidic production of artificial cells (ACs) with reversible permeability
- Homeostatic ACs modulate external and internal pH via chemo-structural feedback
- Prototissues collectively stabilize internal states against external threats
- Inter-AC communication in mixed prototissues counteracts internal threats

Authors

Joshua Krehan, Chuen-Ru Li, Marcos Masukawa, Esther Amstad, Andreas Walther

Correspondence

andreas.walther@uni-mainz.de

In brief

We developed artificial cells (ACs) with homeostatic pH control mechanisms by bringing together pH-modulating enzymes with pH-responsive membranes that cross-couple via chemo-structural feedback. These ACs form prototissues capable of communicating with one another through pH signals and enabling them to collectively adapt to changes in their surroundings to protect functional states and cargos, using homeostatic self-regulation principles.

Krehan et al., 2025, Chem *11*, 102409
June 12, 2025 © 2024 The Author(s). Published by Elsevier Inc.
https://doi.org/10.1016/j.chempr.2024.102409

CellPress

Chem

CellPress
OPEN ACCESS

Article

Homeostatic artificial cells enable self-protection in prototissue spheroids

Joshua Krehan,[1] Chuen-Ru Li,[2] Marcos Masukawa,[1] Esther Amstad,[2] and Andreas Walther[1,3,*]
[1]Life-Like Materials and Systems, Department of Chemistry, University of Mainz, Duesbergweg 10-14, 55128 Mainz, Germany
[2]Soft Materials Laboratory, Institute of Materials, Swiss Federal Institute of Technology in Lausanne (EPFL), 1015 Lausanne, Switzerland
[3]Lead contact
*Correspondence: andreas.walther@uni-mainz.de
https://doi.org/10.1016/j.chempr.2024.102409

THE BIGGER PICTURE Living cells form tissues with specialized functions that maintain homeostasis through feedback-regulated operations. In tissues, cellular communication and collective behavior are crucial for coordinating tasks and ensuring overall functionality. Developing artificial cells (ACs) that can be organized into prototissues to mimic these behaviors is a significant advancement toward creating functional AC systems. These systems are essential for understanding how to design communication networks and collective behaviors, deciphering life's fundamental principles, and advancing biomedical applications. Here, we create AC-based prototissue spheroids that stabilize their microenvironment against external pH threats using a homeostasis mechanism encoded within individual ACs. Like living tissues, these prototissues communicate chemically to collectively resist environmental challenges, paving the way for more advanced artificial tissues in the future.

SUMMARY

Prototissues made from artificial cells (ACs) aim to replicate the behaviors of living tissues, such as communication, collective behavior, and homeostasis. Despite progress in developing diverse AC types, building prototissues and achieving effective communication as well as collective behavior in such prototissues remain challenging. We introduce ACs with an intrinsic homeostatic pH control mechanism that can be organized into prototissues to collectively maintain a stable microenvironment and protect cargo from environmental pH fluctuations. These ACs contain pH-modulating enzymes within a pH-sensitive membrane, allowing for self-regulation through chemo-structural feedback. They adjust pH by importing substrates within a specific pH range and self-regulate to control substrate influx. This enables them to modulate local pH, manage cargo release, and facilitate interactive communication in organized spheroids. Our findings demonstrate the potential of homeostatic ACs to create advanced synthetic tissue mimics, replicating protective and communicative functions of living tissues for biomedical and tissue engineering applications.

INTRODUCTION

Living tissues are heterogeneous structures composed of specialized cells that communicate and exhibit collective behavior within a 3D architecture.[1,2] In nature, intercellular communication and collective behavior are crucial, enabling cells to coordinate actions, respond to environmental changes, and to process chemical information.[3,4] Tissue structures can be mimicked in biomedical organoid research, where multiple cell types are co-organized to better mimic native tissues. The replication of these natural systems from biomimetic artificial cells (ACs) to create synthetic models, known as prototissues, remains a considerable challenge, which encompasses designing ACs with specific functionalities, organizing them into higher-order structures, and devising communication scenarios for emergent prototissue functions.

Recent advances in AC research have focused on diversifying AC structures[5–12] and chemistries. Building upon these developments, individual AC properties and functions, such as growth and replication,[13–16] communication,[17–20] and response to their environment,[21–24] have been realized. Despite progress in creating individual ACs, organizing them on higher length scales remains underexplored. For instance, progress has been made in organizing ACs into prototissues using lipid-[25,26] and DNA-based[27–29] ACs. This has enabled functions such as generating programmable signal processing, biochemical sensing,[25] and DNA-based catalytic functions for chemical communication and adaptation.[27] Achieving such sophisticated organization is

This is an open access article under the CC BY license (http://creativecommons.org/licenses/by/4.0/).

crucial for developing artificial tissues in which ACs work together to replicate the complex functions of living tissues. This capability holds the potential to greatly advance synthetic biology and tissue engineering.

One essential feature of living cells and their tissues is homeostasis, i.e., maintaining a stable microenvironment or functional state despite outside fluctuations.[30] For instance, stable pH levels are crucial for physiological processes and metabolism because many proteins require a constant pH to function optimally.[31] In cells, this is achieved by membrane transporters, respiratory mechanisms, and enzymes. In the synthetic world, enzymatic pH feedback mechanisms offer feedback-regulated and autonomous control over pH.[32] One example is the urease-mediated hydrolysis of urea, which produces ammonia and increases the pH.[33–36] Hard-coded negative feedback based on the bell-shaped activity curve of urease slows down the reaction when pH exceeds 8. Another example is the glucose oxidase (GOx)-glucose system, where GOx converts glucose to gluconic acid (GA), lowering the pH to about 3.6. Both pH feedback reactions offer pathways toward a homeostatic resetting of a pH value when under acidic or basic stress, respectively, and as long as enough substrate or fuel (i.e., urea or glucose) is available. However, the key challenge is to find pathways to regulate excessive fuel conversion, ideally by systems that self-regulate access of the fuel to the catalyst, allowing the enzyme-based pH regulation systems to stop base or acid production at specific values. This requires compartmentalization[37–42] and combination with responsive materials that can shut down fuel uptake. While first systems have been proposed using nanoscale block copolymer aggregates,[43–46] the integration into higher-level tissues and addressing homeostatic functions on such mesoscopic levels remain elusive.

Herein, we introduce self-protection within prototissue AC spheroids by intrinsically homeostatic ACs—with a chemo-structural pH self-regulation mechanism—that collectively maintain a stable microenvironment within the AC spheroid. The ACs are based on enzyme-loaded polymeric microcapsules that precisely sense and adjust both internal and external pH levels to maintain homeostasis. They open or close their shells in response to environmental pH changes, release or uptake small molecules while retaining larger ones inside, and consume external fuel to modulate pH and self-adjust their permeability. We develop two different AC systems: (1) urease-loaded ACs, capable of producing base and equipped with a membrane permeable only at acidic conditions, and (2) GOx-loaded ACs showing inverse behavior by acid production and having a membrane only permeable at high pH. First, we demonstrate how individual ACs precisely modulate the pH, how self-regulation develops via chemo-structural feedback using appropriate membrane design, and how the system speed can be fine-tuned. Next, we show how urease-ACs organized in spheroid-type prototissues can protect cargo in the spheroid interior from environmental pH changes by collectively maintaining a stable pH microenvironment. Finally, we demonstrate how mixtures of urease-ACs and GOx-ACs communicate through pH signals within a synthetic multi-AC prototissue composed of two different ACs. We envision that our system could pave the way for the development of advanced synthetic tissues that mimic the protective and communicative functionalities of living tissues.

RESULTS AND DISCUSSION

System design for homeostatic ACs

We fabricated our homeostatic ACs from enzyme-loaded polymeric microcapsules through microfluidics using water-oil-water (w/o/w) double emulsion formed through a double cross-junction microfluidic chip[47] and subsequent photopolymerization (Figures 1A and S1). The w/o/w double emulsions consist of an inner aqueous enzyme solution enclosed in an oil shell containing monomers, crosslinker, and photoinitiator. Our design includes two distinct AC types: (1) urease-loaded ACs with a weak, pH-responsive polycation shell and (2) GOx-loaded ACs with a weak, pH-responsive polyanion shell. Both feature pH responsiveness and reversible permeability.

We designed two polycationic ACs based on polymethacrylate shells with tertiary amine groups, in which the alkyl chains attached to the amine influence the pH responsiveness via the p*K*a value. Specifically, we use the monomer 2-(diethylamino) ethyl methacrylate yielding poly(2-(diethylamino)ethyl methacrylate) (PDEAEMA) shells or 2-(diisopropylamino)ethyl methacrylate yielding poly(2-(diisopropylamino)ethyl methacrylate) (PDiPAEMA) shells (Figure 1A, middle frame). Additionally, we adapted a system by Weitz and co-workers for polyanionic ACs with pH-responsive carboxyl groups based on hydrolysis of poly(methacrylic anhydride) (PMAAn) shells.[48] We optimized the hydrolysis step and increased the hydrophobicity of the resulting shell by using *n*-butylamine during the hydrolysis, allowing completion of the reaction within 1 h and resulting in poly(methacrylic acid-*co*-N-butylmethacrylamide) (simplified as PMAA) ACs (Figure 1A, right frame). The shell thickness of all ACs is 1–2 μm in the collapsed state, increasing by 1.5-fold for PDEAEMA and PDiPAEMA ACs and by 3.5-fold for PMAA ACs in the swollen state (Figure S2C).

The polycationic ACs exhibit reversible swelling in acidic conditions, controlled by the pK_a of the amine groups (Figure 1B). Below a pH of 6.9 for PDEAEMA or 5.6 for PDiPAEMA, protonation of the amine groups to quaternary ammonium renders the shell hydrophilic, swollen, and permeable to small molecules while retaining the larger enzyme urease inside. Deprotonation returns the shell to its hydrophobic and impermeable state. When urea diffuses through the swollen membrane, urease catalyzes the conversion of urea to ammonia and CO_2. Ammonia raises the local pH inside and around the ACs. This system thereby self-regulates by a negative chemo-structural feedback loop in which the shell closes above the specific pH for shell collapse (6.9 or 5.6), preventing further uptake of urea and thus completely arresting the reaction inside the AC. This prevents uncontrolled pH elevation as for unencapsulated urease (pH profile in Figure 1B). The p*K*a value controls the closure pH. In contrast, polyanionic ACs with pH-responsive carboxyl groups exhibit inverse swelling-shrinking behavior (Figure 1C). Above pH 4.6, deprotonated carboxylates render the shell permeable to glucose, whereas below pH 4.6, protonated carboxyl groups make the shell impermeable to glucose. When glucose diffuses inside the AC, GOx converts it to GA, decreasing the local pH.

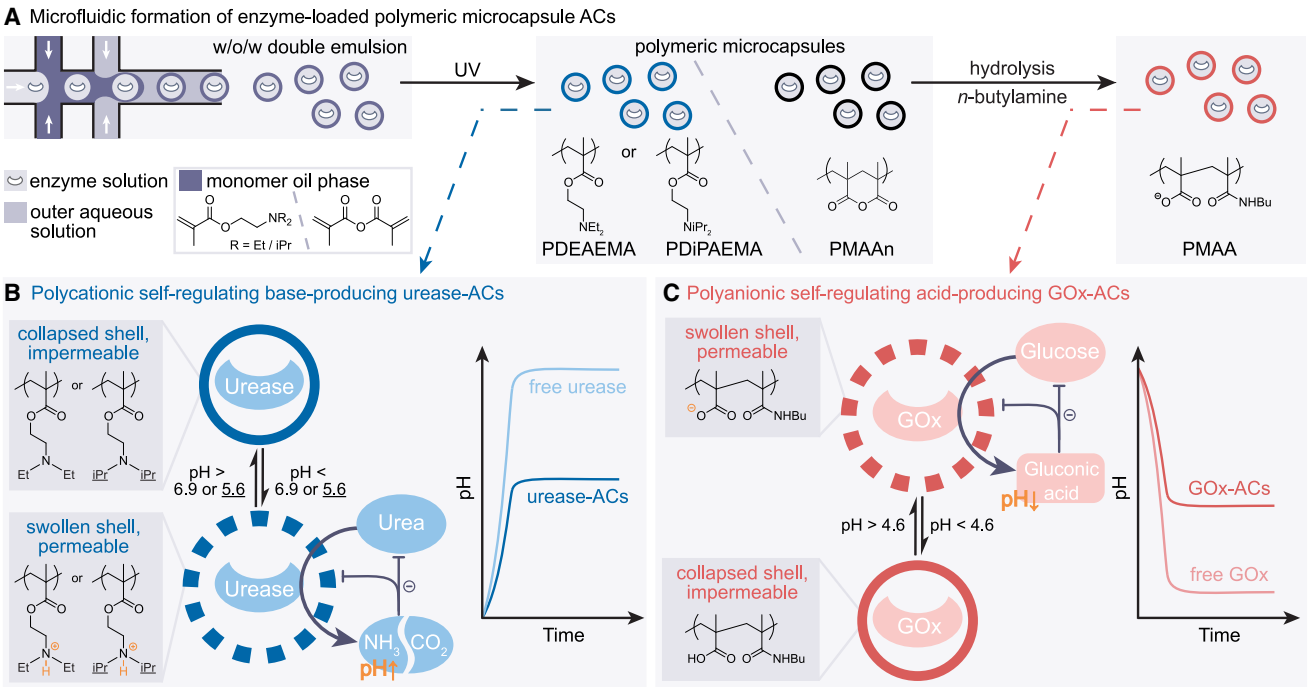

Figure 1. Fabrication and operational principles of pH modulation of homeostatic ACs

(A) Microfluidic formation of enzyme-loaded polymeric microcapsule ACs from w/o/w double emulsions followed by photopolymerization.

(B) Self-regulating behavior of polycationic urease-ACs, showing reversible permeability and base production at pH < 6.9 (PDEAEMA) or < 5.6 (PDiPAEMA).

(C) Self-regulating behavior of polyanionic GOx-ACs, illustrating reversible permeability and acid production above pH 4.6.

The concomitant protonation of carboxyl groups closes the shell below pH 4.6, manifesting the chemo-structural feedback.

In summary, this fabrication platform allows for the scalable synthesis of homogeneous pH-homeostatic ACs that can sense the pH, process a chemical fuel, and actuate the surrounding pH to modulate their microenvironment and the membrane to self-regulate permeability. They maintain homeostasis by adjusting the internal and external pH back to a specific value. Furthermore, these ACs selectively regulate the entry and exit of substances through the membrane based on molecular weight. Small molecules such as chemical fuels can transition only in the swollen state, whereas larger molecules such as fuel processors (urease, GOx) are permanently confined within the internal environment, distinct from the external milieu.

Swelling-shrinking behavior of pH-responsive ACs

We first discuss the pH-dependent swelling and permeability behavior of our different ACs. The ACs exhibit size changes as a function of pH depending on their polymer composition (Figure 2). PDEAEMA and PDiPAEMA ACs swell in acidic pH, while PMAA ACs swell inversely in basic pH. Specifically, PDEAEMA ACs increase in diameter by 27%, expanding from 44 to 56 μm, when the pH drops below 6.9 (Figure 2A). Similarly, PDiPAEMA ACs swell by 63% below pH 5.6, expanding from 41 to 67 μm. This larger swelling of PDiPAEMA ACs stems from their more hydrophobic isopropyl groups that retain less water in the collapsed high pH state, compared with PDEAEMA. Notably, the change in diameter for both PDEAEMA and PDiPAEMA ACs occurs abruptly, indicating that the shell changes polarity within a very narrow pH range. The swelling-shrinking behavior of the ACs is reversible, as exemplified for PDEAEMA ACs over five pH cycles in Figure 2B and for PDiPAEMA ACs as well as PMAA ACs in Figure S2. This is a relevant feature for consistent and robust pH modulation. In contrast, PMAA ACs show inverted swelling behavior with a slightly broader switching window centered around pH 6.2. The total size increase is 39% with a diameter change from 56 to 78 μm when the pH is increased (Figures 2C and S2D).

To correlate the permeability of these ACs with their swelling behavior, we encapsulated rhodamine 6G (R6G) inside the polycationic ACs and monitored the release at different pH through wide-field fluorescence microscopy (Figures 2D and 2E). Both PDEAEMA and PDiPAEMA ACs release the dye completely, only after the pH drops to their respective swelling pH of 6.9 and 5.6. At high pH, both ACs retain the dye and thus their impermeable state for at least 2 months. In contrast, PMAA ACs swell and release R6G upon hydrolysis at neutral pH (Figure S2D).

In addition, we conducted a molecular weight cutoff analysis for the ACs at various pH, using fluorescently labeled dextrans and PEGs ranging from 5 to 70 kDa, as well as small dye molecules (Figure S3). In the swollen state, PDEAEMA and PDiPAEMA ACs are impermeable to 10 kDa dextrans, while 5 kDa PEG and dyes can pass through the membrane. In the collapsed state, even dyes cannot permeate through the membrane. PMAA ACs behave similarly but with a higher molecular weight cutoff. They are impermeable to 70 kDa dextrans across

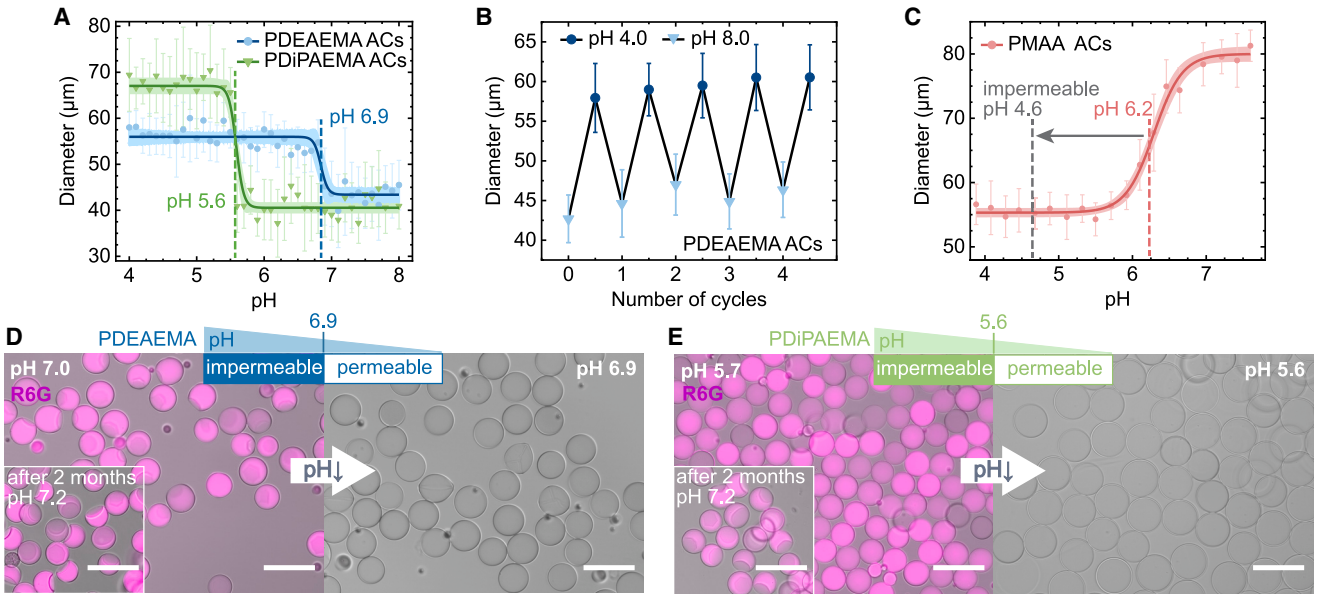

Figure 2. Swelling-shrinking behavior and permeability of homeostatic ACs

(A) Diameter of PDEAEMA and PDiPAEMA ACs at varying pH levels. Each pH was adjusted with a suitable buffer of 100 mM buffer capacity. Data points represent the average diameter of 50 ACs, with error bars representing the standard deviation and a sigmoidal fit and 95% confidence band as shaded contours.

(B) Reversible swelling and shrinking of PDEAEMA ACs across five pH cycles (pH 8.0 to 4.0). Error bars indicate the standard deviation (n = 50 ACs).

(C) Diameter changes in PMAA ACs (n = 40 ACs) across different pH levels, presented with error bars representing the standard deviation and a sigmoidal fit and 95% confidence band in shaded contours. The gray dashed line indicates the pH below which PMAA ACs are impermeable to glucose (see also Figure 3D). Each pH was adjusted with a suitable buffer of 100 mM buffer capacity.

(D and E) Fluorescence wide-field images showing permeability of (D) PDEAEMA and (E) PDiPAEMA ACs with encapsulated R6G at different pH levels. Both ACs release R6G completely below their respective transition pH (6.9 for PDEAEMA and 5.6 for PDiPAEMA) and retain R6G above it. Scale bars: 100 μm.

all pH, whereas 20 kDa dextran and dyes can only not permeate through the collapsed membrane. This demonstrates that the shell has desired permeability features, i.e., enzymes such as urease (M = 544 kDa) and GOx (M = 160 kDa) remain encapsulated within the ACs even in the swollen state, while small molecules can only transition into the ACs in the swollen state.

pH modulation capabilities and homeostatic AC behavior

We next turn to understanding the self-regulating, homeostatic nature of our pH-sensitive ACs encapsulating pH-modulating enzymes on account of the developing chemo-structural feedback. Figure 3 illustrates the pH modulation capabilities of our homeostatic ACs. When urea or glucose is added as a fuel, these substrates permeate through the swollen membrane, triggering the production of either base or acid until the pH feedback closes the shell upon reaching a specific pH value (Figures 3A and 3B). This mechanism contrasts with the unregulated pH changes of the free enzymes. Free urease shows a pH increase from 4.5 to 8.5 (Figure 3C). Conversely, PDEAEMA urease-ACs raise the pH from 4.5 to only 7.1 (Figures 3B and 3C), slightly exceeding the permeability pH of 6.9 for R6G. The higher pH likely results from the smaller, non-charged urea diffusing more easily through the shell than R6G. Similarly, PDiPAEMA urease-ACs elevate the pH to a final value of 5.6, precisely matching the permeability pH of R6G. The GOx-glucose system exhibits an inverse pH profile (Figure 3D). Starting at pH 7.4, free GOx decreases the pH to 3.4, whereas GOx-ACs lower the pH to only 4.6, whereafter additional glucose can no longer enter the AC to find its enzyme processor. Notably, this pH is significantly lower than the swelling threshold of pH 6.2. This is due to the gradual protonation of carboxyl groups that inhibit glucose diffusion only below pH 4.6. Acid production speeds up below pH 6.0 because the buffering capacity of carboxyl groups has been overcome, and because the enzyme itself has a positive chemical feedback with an optimum activity around a pH of 5.5.[42,49] For all AC types, the pH values reach a well-developed plateau pH, confirming that the pH modulation system not only slows down but completely halts acid or base production at the target pH. Both ACs can enter fully dormant states in their closed states, which is an important prerequisite for homeostatic resetting and communication scenarios. Notably, all experiments began with a substrate concentration of 100 mM, and one full pH modulation cycle by PDEAEMA urease-ACs consumes 39 ± 2 mM urea (leaving 61 ± 2 mM urea), while PDiPAEMA consumes 32 ± 2 mM urea (leaving 68 ± 2 mM). PMAA consumes 59 ± 3 mM glucose, leaving 41 ± 3 mM at the end of a cycle. From now on, we will focus solely on PDEAEMA and PMAA, as PDiPAEMA shows qualitatively similar behavior to PDEAEMA.

The pH modulation speed can be tuned by varying the AC concentration, the concentration of encapsulated enzyme, and the fuel concentration (Figures 3E–3G and 3I–3K). For PDEAEMA urease-ACs (1 g/L urease), increasing the number of ACs accelerates pH elevation. The time required to raise the pH from 5.0 to

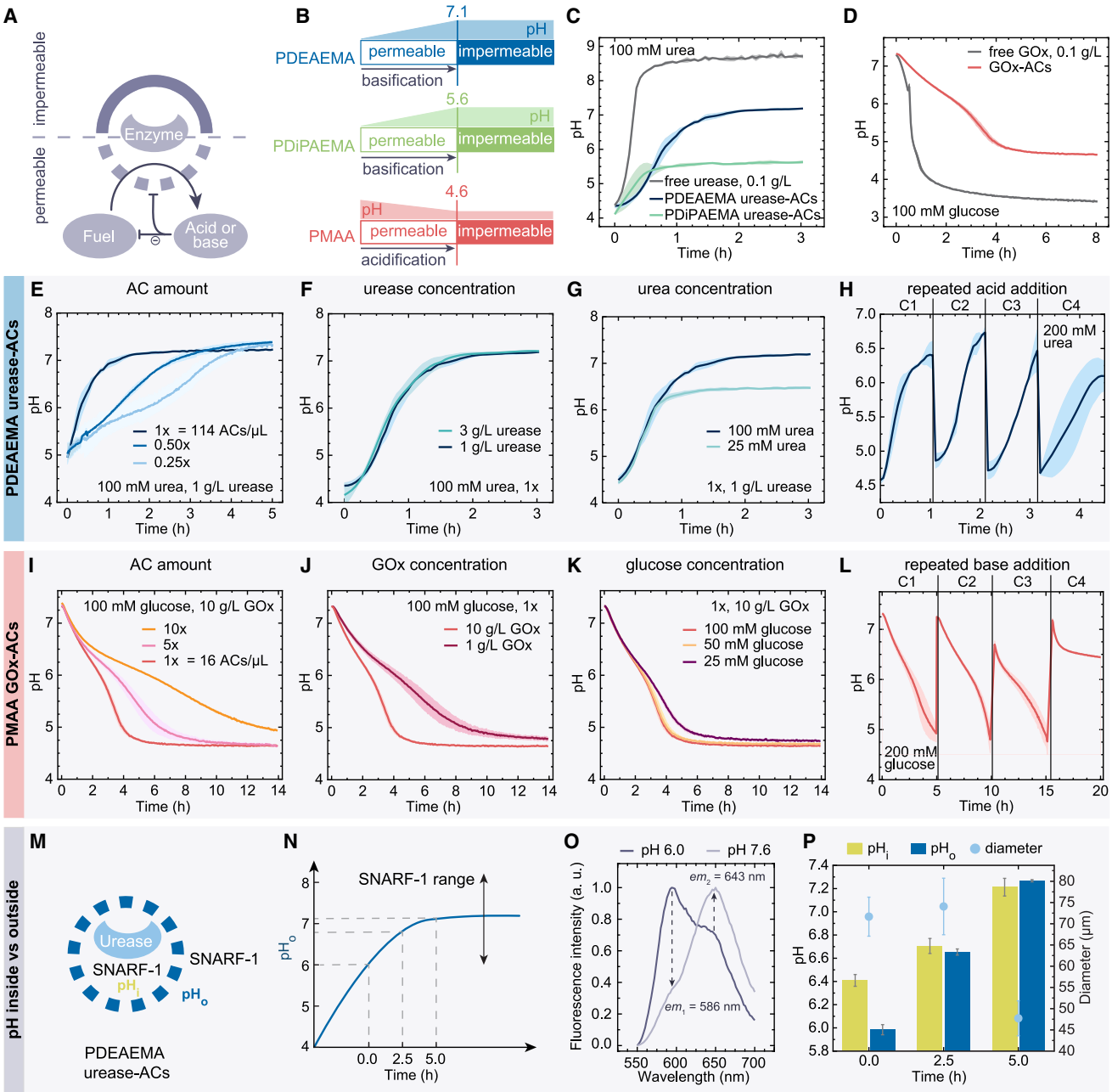

Figure 3. pH modulation capabilities and homeostatic behavior

The pH profiles represent an average contribution of *n* independent measurements, and the shaded contours depict the standard deviation.

(A–E) (A) Schematic of self-regulation in ACs and (B) pH modulation of enzyme-loaded ACs. (C) pH profile comparison between free urease and (D) GOx in comparison with the respective ACs. $n = 3$. Effects on pH modulation for PDEAEMA urease-ACs: (E) AC amount x, with 1x = 114 ACs/μL. 0.25x, 0.5x: $n = 2$; 1x: $n = 3$.

(F) Variation of urease concentration within the ACs. $n = 3$.

(G) Effect of urea concentration added to the medium. 100 mM: $n = 3$; 25 mM: $n = 2$.

(H and I) Repeated acid addition (0.25 M HCl) of cycles C demonstrating repeated pH modulation for PDEAEMA urease-ACs. 1x (114 ACs/μL) AC amount, 1 g/L urease encapsulated; $n = 2$. Effects on pH modulation for PMAA GOx-ACs: (I) AC amount x, with 1x = 16 ACs/μL. $n = 3$.

(J) Variation of GOx concentration within the ACs. $n = 3$.

(K) Effect of glucose concentration added to the medium. $n = 3$.

(L) Repeated acid addition (0.25 M NaOH) demonstrating repeated pH modulation for PMAA GOx-ACs. 1x (16 ACs/μL) AC amount, 10 g/L GOx encapsulated; $n = 2$.

(legend continued on next page)

7.1 changes from 1 via 3 to 4 h in a dilution series from 1x (114 ACs/μL) to 0.5x (57 ACs/μL), and 0.25x (29 ACs/μL) (Figure 3E). Interestingly, GOx-ACs (10 g/L GOx) show a somewhat different effect. They exhibit a buffering effect, where higher AC concentrations slow the acidification process due to the gradual protonation of the carboxyl groups before reaching the final pH of 4.6 (Figure 3I). The 1x concentration (16 ACs/μL) reaches pH 4.6 in 6 h, while 5x (80 ACs/μL) requires 10 h, and 10x (160 ACs/μL) achieves only pH 5.1 after 14 h. This effect originates from the balance between how much enzyme can be encapsulated in comparison with the membrane thickness, where the latter follows some fabrication constraints to reach a stable microfluidic production.

Increasing the urease concentration from 1 to 3 g/L inside urease-ACs does not affect the speed of basification at constant urea concentration (100 mM urea, Figure 3F). This indicates that diffusion limitations of urea and basic products through the membrane dominate the system. However, increasing the GOx concentration from 1 to 10 g/L inside GOx-ACs accelerates acid production, reducing the time to reach pH 4.6 from over 14 to 6 h (100 mM glucose, Figure 3J). Changes in the fuel concentration in a reasonable window to expect sufficient pH changes do not affect the base- or acid-production rate at concentrations above 25 mM for both systems. Urease-ACs exhibit similar pH increases for 100 and 25 mM urea within the first half-hour, confirming the diffusion-limited behavior of the system (Figure 3G). However, 25 mM urea only allows for an increase of the pH to 6.5 because the fuel amount is insufficient to deprotonate all ammonium groups in the membrane. For GOx-ACs, glucose concentrations of 100 and 50 mM yield comparable pH changes, while the pH drop is slightly slower for the lowest concentration of 25 mM glucose, which approaches the Michaelis-Menten constant $K_{m,GOx} \approx 22$ mM (Figure 3K; for comparison $K_{m,urease} \approx 2.5$ mM).

To demonstrate the ability of our homeostatic ACs to undergo multiple pH resetting cycles, we charged a urease-AC system (114 ACs/μL, 1 g/L urease) with a high amount of 200 mM urea, and we injected HCl at multiple time points to reset the pH to low pH after the urease-ACs had leveled the pH to near the fully closed state. Indeed, multiple cycles can be achieved, confirming the efficient chemo-structural feedback that closes the urease-AC against urea permeation at high pH (Figure 3H). The last cycle (C4) only increases to a moderate pH, because the system has run out of the background fuel urea. For GOx-ACs (16 ACs/μL, 10 g/L GOx), we inverted the system and performed multiple injections of NaOH to increase the pH from near the fully closed state. A similar cycling behavior can be observed, again with a noticeably slower behavior in the last cycle (Figure 3L). This confirms that both AC types can exploit their dormant to active switch repeatedly to act as homoeostatic resetting units in a background fuel situation.

Next, we turn to the intriguing question of to what extent the pH change inside the AC may outpace the pH change in the environment (Figures 3M–3P). We selected the polycationic PDEAEMA ACs because suitable pH-sensing dyes are available to monitor this behavior with a confocal laser scanning microscope (CLSM). To this end, we encapsulated the pH-sensing dye SNARF-1-Dex (70 kDa) inside PDEAEMA urease-ACs (1 g/L urease; 29 ACs/μL) and added the same concentration to the external solution to simultaneously monitor pH inside (pH_i) and pH outside (pH_o) (Figures 3M, 3N, and S4). SNARF-1 emits fluorescence at two distinct wavelengths, with their intensities depending on the pH (Figure 3O). The ratio of these emission intensities can track pH between 6.0 and 8.5. Starting with ACs at pH 6.0, we added 100 mM urea and monitored both the fluorescence change and the AC diameter to simultaneously follow pH development and AC swelling ($t = 0$ h; Figure 3P). Right after the addition of urea, the pH_o is 6.0 whereas the pH_i is slightly higher at 6.4 (Figure 3P), indicating fast NH_4OH generation from urea by urease within the ACs. The AC diameter stays stable for the first 2.5 h, during which pH_o increases to 6.6 and pH_i to 6.7, suggesting an ongoing equilibration between pH_i and pH_o. After 5 h, the ACs shrink to 48 μm, marking the stop of urease operation. The pH_o and pH_i converge to approximately the same pH of 7.3 and 7.2, respectively. Color-mapped pH visualizations in Figure S5 support these findings. This behavior correlates relatively well with the switching pH of the PDEAEMA AC. Taken together, at early stages close to $t = 0$ h, the produced NH_4OH first needs to establish a steady-state equilibrium at the membrane where substantial amounts of base are consumed at the protonated membrane material, balancing the outer acid concentration. As pH increases, the balance shifts and the pH imbalance goes to zero. This also confirms that NH_4OH can fully permeate and equilibrate through the membrane because there is no rise of pH_i to 8.5 as would be the case for free urease in solution. The chemo-structural feedback and self-regulated closure thus stem primarily from preventing further influx of urea and not outflux of NH_4OH.

Self-protection of individual homeostatic ACs

Before turning to communicating systems in prototissues, we first demonstrate simple self-protection features on an individual AC level. To this end, we raise the question of whether our homeostatic ACs can protect their interior against occurring acidification or basification in their surroundings by generating an internal counteraction. For PDEAEMA urease-ACs, we realized such a system by introducing glucono delta-lactone (GDL), which slowly hydrolyzes into GA to lower the pH[50], to the dormant state of such ACs at high pH and in the presence of 100 mM urea (Figure 4A). Note that GA is a relatively strong

(M) Schematic of the pH-sensitive fluorescent dye SNARF-1-Dex (70 kDa) inside and outside of PDEAEMA urease-ACs for monitoring the pH inside (pH_i) and outside (pH_o) simultaneously.
(N) Schematic for pH_o changes over time with the range in which SNARF-1 can operate (pH 6.0–8.5).
(O) Fluorescence emission spectra of SNARF-1 at pH 6.0 and 7.6.
(P) Correlation of AC diameter with pH changes inside and outside PDEAEMA urease-ACs over time. The pH was calculated from the fluorescence intensity of SNARF-1 (ex = 561 nm; em_1 = 565–595 nm, em_2 = 625–655 nm), as measured from CLSM images in $n = 3$ different areas inside and outside the ACs. The error bars indicate the standard deviation. $n = 15$ for the diameter of individual ACs. AC concentration of 0.25x (29 ACs/μL, 100 mM urea, 1 g/L urease encapsulated).

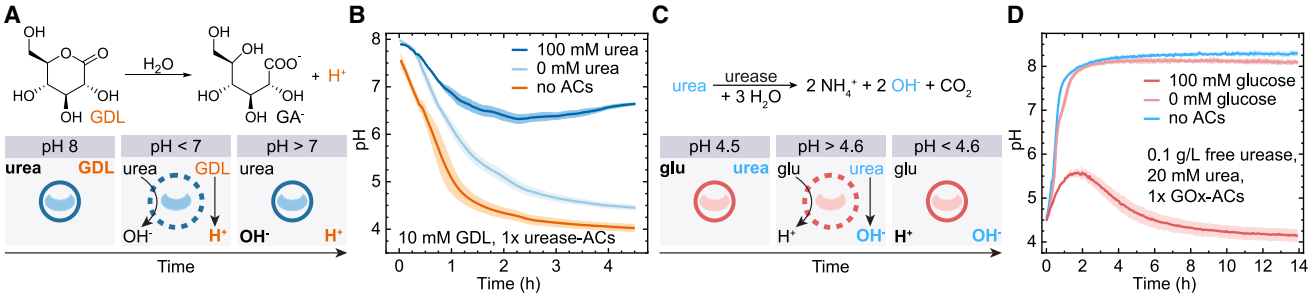

Figure 4. pH stabilization by homeostatic ACs in response to external acid or base generation

(A) GDL hydrolysis to GA creates an acidic environment. PDEAEMA urease-ACs swell below pH 7, producing hydroxide ions to stabilize pH around 7.

(B) pH profile with 10 mM GDL with pH feedback (100 mM urea) and without pH feedback (0 mM urea), compared with GDL only. 1x urease-ACs (114 ACs/μL) with 1 g/L urease encapsulated were added. Shaded contours represent the standard deviation of two individual experiments.

(C) Schematic for GOx-ACs with external urease-urea system: the ACs stabilize the pH at 4.6.

(D) pH changes with 0.1 g/L urease and 20 mM urea with feedback (100 mM glucose) and without pH feedback (0 mM glucose), compared with the urease-urea system only. 1x GOx-ACs (16 ACs/μL) with 10 g/L GOx encapsulated were added. Shaded contours represent the standard deviation of three individual experiments.

acid with a pK_a of 3.86. Initially, at a pH of 8, the ACs remain impermeable, preventing urea from diffusing through the membrane (Figure 4A, left). As the pH decreases below 7.0 due to GDL hydrolysis, the ACs swell and provide pH feedback. Urea diffuses through the membrane and is converted to NH_4OH by urease. This pH feedback counters the acidification by GDL and stabilizes the pH around 7 (Figure 4A, middle). Once all GDL is hydrolyzed and no more H^+ is produced, the ACs close at approximately pH 7. Figure 4B confirms this behavior: 10 mM GDL without urease-ACs lowers the pH to 4.0 after 4 h, whereas 10 mM GDL with AC pH feedback (100 mM urea) maintains the pH just below 7 for the same duration. A control of 10 mM GDL with urease-ACs but without urea reduces the pH to 4.5, which is slightly higher compared with pure GDL because of the protonation of amine groups in the AC shell by GA (buffer capacity). Similarly, we tested GOx-ACs using an environmental basification system based on urease-urea to generate NH_4OH outside the ACs (Figure 4C). Starting at a pH of 4.5, urea was added to initiate NH_4OH production (Figure 4C). Once sufficient pH pressure develops on the outside, the ACs open above pH 4.6 to permit glucose diffusion, which then produces GA to counter the pH increase, eventually stabilizing the environment at pH 4.6. Figure 4D shows that the urease-urea system first raises the pH to 5.5 within 2 h, but then GOx-ACs lower the pH back to 4.6 after 6 h, where it remains stable. In contrast, without pH feedback (no ACs or ACs without glucose), the pH rapidly increases to 8.2 within 2 h, where it plateaus. These examples demonstrate efficient self-protection features to potentially prevent cargo leakage and maintain pH stasis.

Self-protection within spheroidal prototissues by homeostatic urease-ACs

Next, we assemble spheroid-type prototissues from urease-ACs and introduce a spatially orchestrated self-protection mechanism. These AC spheroids can protect their internal ACs as a collective from environmental pH "threats" by collectively maintaining a stable microenvironment within the spheroid core (Figure 5). We formed the AC spheroids by mixing PDEAEMA urease-ACs (1 g/L urease) with sulfonic acid-functionalized polystyrene beads (PS-SO_3H beads; diameter = 5 μm) in a ca 1:20 ratio. The negatively charged PS-SO_3H beads bind to the positively charged polycationic ACs via electrostatic interactions, resulting in spheroids approximately 2 mm in diameter (Figure 5B). To illustrate the formation of a distinct microenvironment within the AC spheroids and demonstrate the self-protection feature, we encapsulated the dyes R6G and fluorescein-labeled dextran (FITC-Dex, 500 kDa) inside the urease-ACs (Figure 5A). R6G serves as a model cargo that requires protection from environmental pH changes, leaking out when the ACs swell below pH 6.9, while the larger FITC-Dex remains inside and simplifies imaging as well as allows for tracing of pH development, as FITC turns less fluorescent at low pH. Building on our understanding of individual ACs (Figure 4), we simulated an environmental threat by adding GDL to lower the pH over time. We discuss two scenarios: (1) without pH feedback for urease-ACs without urea in the environment and (2) with pH feedback for urease-ACs having urea in the environment. Without pH feedback, GA produced by GDL migrates into the spheroid, lowers the pH, and causes all ACs to swell and release their R6G cargo. The system fails to protect against loss of cargo (Figure 5B, middle). However, in the presence of 100 mM urea, only the outermost ACs swell (2–3 layers) and lose their cargo, whereas their efficient NH_4OH production prevents a further influx of the GA from the environment (Figure 5B, right). Consequently, the ACs work together to create a controlled microenvironment where the pH is maintained above 7 so that the ACs within the spheroid core are protected from swelling and cargo loss.

Fluorescent wide-field microscopy illustrates these findings (Figures 5C–5F). In the non-protected scenario, R6G leaks out fully after 18 h (Figure 5D), and the fluorescence intensity of FITC-Dex decreases, confirming a pH drop inside the ACs. CLSM allows for characterizing the diameter of individual ACs (Figures 5H and 5I). All ACs are swollen across the entire spheroid (yellow line in Figure 5I), and the diameter increases from 45 to 68 μm, resulting in an overall increase of the spheroid area by around 76% (yellow bar in Figure 5J). Conversely, in the

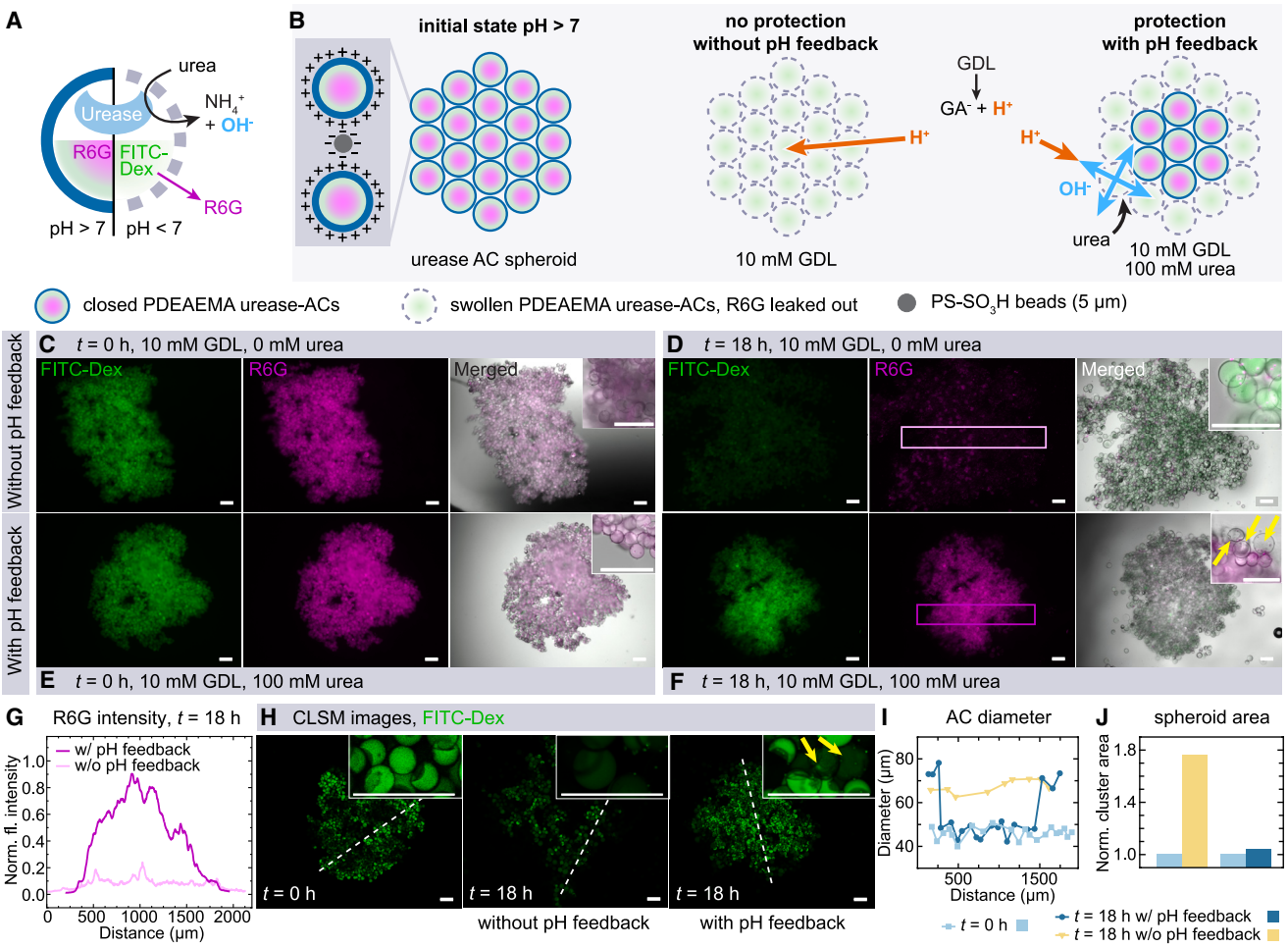

Figure 5. Collective self-protection in AC spheroids

(A) Schematic of PDEAEMA urease-ACs encapsulating R6G and FITC-Dex (500 kDa), with pH-dependent permeability.

(B) Formation and behavior of PDEAEMA AC spheroids: initial state at pH > 7, no protection without pH feedback (w/o), and protection with pH feedback (w/). 10 mM GDL was added as an external pH threat.

(C–F) (C and D) Fluorescence wide-field images of spheroids without pH feedback that fully leak their dye R6G, whereas (E and F) spheroids with pH feedback protect the dye against release in the AC spheroid core. The AC spheroids in (C) and (D) represent the same spheroid as in (E) and (F). Scale bars: 200 μm.

(G) Normalized fluorescence intensity of R6G at t = 18 h with and without pH feedback. The fluorescence was measured from the rectangular boxes in (D) and (F).

(H) CLSM images of FITC-Dex at t = 0 and 18 h without and with pH feedback. Scale bars: 200 μm. Fluorescence of FITC weakens drastically for the non-protected case, whereas only a few outer urease-ACs turn non-fluorescent for the protected case.

(I) Urease-AC diameter analysis across spheroids. Swelling takes place only in the outer regions in the protected case (dark blue), whereas swelling occurs across the entire spheroid in the non-protected case (yellow line). Diameters were calculated from CLSM images in (H) along the dashed line.

(J) Comparison of spheroid area increase from t = 0 to 18 h without and with pH feedback. The total spheroid area was measured from wide-field images in (C)–(F).

self-protected AC spheroids, most of the cargo R6G remains inside the AC spheroid, as seen in the fluorescent wide-field images (Figures 5E and 5F). Additionally, the cross-section analysis of the fluorescence intensity of protected and non-protected spheroids shows a significantly higher intensity for the protected spheroid (wide-field imaging; Figure 5G). Notably, the close-up image shows that only a few ACs are swollen in the outermost layers of the self-protected spheroid. Those outermost urease-ACs have lost their R6G cargo but efficiently protect the other ACs (yellow arrows, t = 18 h; Figures 5F and 5H). CLSM quantifies the size increase of the ACs at the periphery as seen in the dark blue line in Figure 5I. Consequently, the spheroid area increases only by around 4% (dark blue bar; Figure 5J). Overall, this demonstrates a highly efficient self-protection function that only operates in the collective ensemble of the spheroid assembly. A duplicate of this experiment can be found in Figure S6. The self-protection within the AC spheroids fails at a higher GDL concentration of 20 mM because the acidification occurs about two times faster, compared with 10 mM (Figure S7).

Communication between urease-ACs and GOx-ACs through pH signals in multi-AC spheroids

In biomaterials research, organoids are distinguished from spheroids by having multiple cell types arranged within the

assembled structure and typically resembling the first steps toward a functional organ. Taking inspiration from this concept, i.e., the involvement of more than one cell type, we designed multi-AC prototissues that combine urease-ACs and GOx-ACs (Figure 6). Our approach is to establish feedback-regulated communication between both ACs through pH signals, which trigger a self-protection mechanism. To demonstrate this, we incorporated GOx-ACs (10 g/L GOx) into urease-AC (1 g/L urease) spheroids in a ratio of 1:10. This enables the GOx-ACs to act as an internal acid source (threat) within the AC spheroid (Figure 6A). Starting at pH > 7, and after supplying the system with the relevant environmental fuels (glucose, urea), glucose (25 mM) diffuses into the multi-AC spheroids and subsequently into the swollen GOx-ACs (Figure 6B). Therein it is converted into GA by GOx, thus lowering the pH around the GOx-ACs. Without urea (100 mM), no pH feedback is provided, causing all the urease-ACs in the AC spheroid to swell and release their cargo R6G (Figure 6B, middle). However, in the presence of urea, the nearby urease-ACs sense the locally generated pH signal, open their gates to allow for an influx or urea, and thereby give counter-pH feedback (Figure 6B, right). This leads to an efficient self-protection function that can even balance out in-spheroid-produced pH threats. Consequently, only the urease-ACs close to the GOx-ACs react to the pH change by swelling, while the others remain closed, protecting their cargo.

Figures 6C–6F display fluorescent wide-field images, and Figures 6G and 6H offer close-up CLSM images for better visualization. The GOx-ACs are labeled with an $Alexa_{700}$-Dex. We first discuss the control: without urea in the environment, all urease-ACs in the spheroid swell after 18 h upon glucose addition (Figures 6C and 6D). This is shown by an increase in the size of all ACs (yellow line; Figure 6K) calculated from CLSM images along the dashed line (Figure 6J). This swelling leads to a ca 50% increase in the spheroid area (yellow bar; Figure 6L). Close-up CLSM images reveal the complete leakage of R6G from urease-ACs, while FITC-Dex remains inside but with lower intensity due to the lowered pH (Figure 6G). Figure S8 presents the enlarged close-up images, providing a more detailed view of the fluorescence intensity changes. Notably, R6G accumulates within the negatively charged PMAA shell, maintaining significant fluorescence intensity detectable through wide-field microscopy (Figures 6D, 6G, and S8). Additionally, R6G tends to localize with the small SO_3-PS beads used to assemble the multi-AC spheroids. In contrast, if 100 mM urea is present in the environment, the urease-ACs respond to the pH signal from the GOx-ACs and rapidly shut down acidification. Some urease-ACs near GOx-ACs respond to the pH decrease by swelling, as indicated by the yellow arrows in the close-up CLSM images (Figure 6I). Those selectively responding urease-ACs also show up as peaks in the cross-sectional size analysis in Figure 6K (blue line). All other urease-ACs are sufficiently protected, do not swell, and do not leak their cargo R6G (Figures 6E and 6H). The spheroid area increases only slightly by around 12% (dark blue bar, Figure 6L). Again, it becomes evident that the trace amounts of R6G that are leaked from the urease-ACs that opened to protect the others are localized to the SO_3-PS-beads. A duplicate of this experiment can be found in Figure S9. Notably, the self-protection within the AC spheroids fails at a urease-AC:GOx-AC ratio of 1:1 (Figure S10).

Conclusions

In summary, we presented the first self-protection mechanisms in prototissue spheroids organized by homeostatic ACs that maintain a stable microenvironment through collective behavior. These ACs can accurately sense and adjust both internal and external pH levels to sustain homeostatic regulation. They function by opening or closing their shells in response to environmental pH changes, allowing the release or uptake of small molecules, while retaining larger ones inside. The ACs are made up of pH-responsive polymeric shells that are reversibly permeable. We developed two distinct AC systems: urease-loaded ACs that produce base and GOx-loaded ACs that generate acid. Initially, we showed how free ACs precisely modulate pH and how the speed of pH modulation can be tuned using various parameters. The integrated pH feedback loop ensures that the shells become impermeable once a desired pH is achieved, thus self-regulating the system to a specific pH value by chemo-structural feedback principles. Next, we demonstrated that urease-ACs can organize into spheroidal prototissue and protect cargo within the spheroid from environmental pH changes by collectively maintaining a stable pH microenvironment, giving rise to a self-protection function and preventing leakage of small cargoes. Finally, we illustrated that urease-ACs and GOx-ACs can communicate within a co-spheroid through pH signals, which allows for even internal pH threats to be counterbalanced locally. While we showcased protection against leakage, the systems may very well be expanded to more complex functions. In essence, the systems effectively transduce homeostatic behavior from an individual AC level to a collective homeostatic protection function in synthetic tissue mimics.

Our AC spheroids represent a significant advancement in developing biomimetic artificial tissues. To further advance this research, future studies will explore additional aspects such as pH monitoring within the microenvironment or the investigation of different communication mechanisms between various types of ACs. Additionally, our homeostatic AC platform holds promise for applications as metabolic support systems in biomaterials application, including the field of tumor immunology, where maintaining an immune-supportive environment requires counteracting the acidification induced by tumors.[51] By addressing acid-driven macrophage polarization and supporting cytotoxic T cell function, this approach could aid in overcoming tumor immunoevasion, which remains a major challenge in immunotherapy.

METHODS

Details regarding the methods can be found in the supplemental methods.

RESOURCE AVAILABILITY

Lead contact

Further information and requests for resources should be directed to and will be fulfilled by the lead contact, Andreas Walther (andreas.walther@uni-mainz.de).

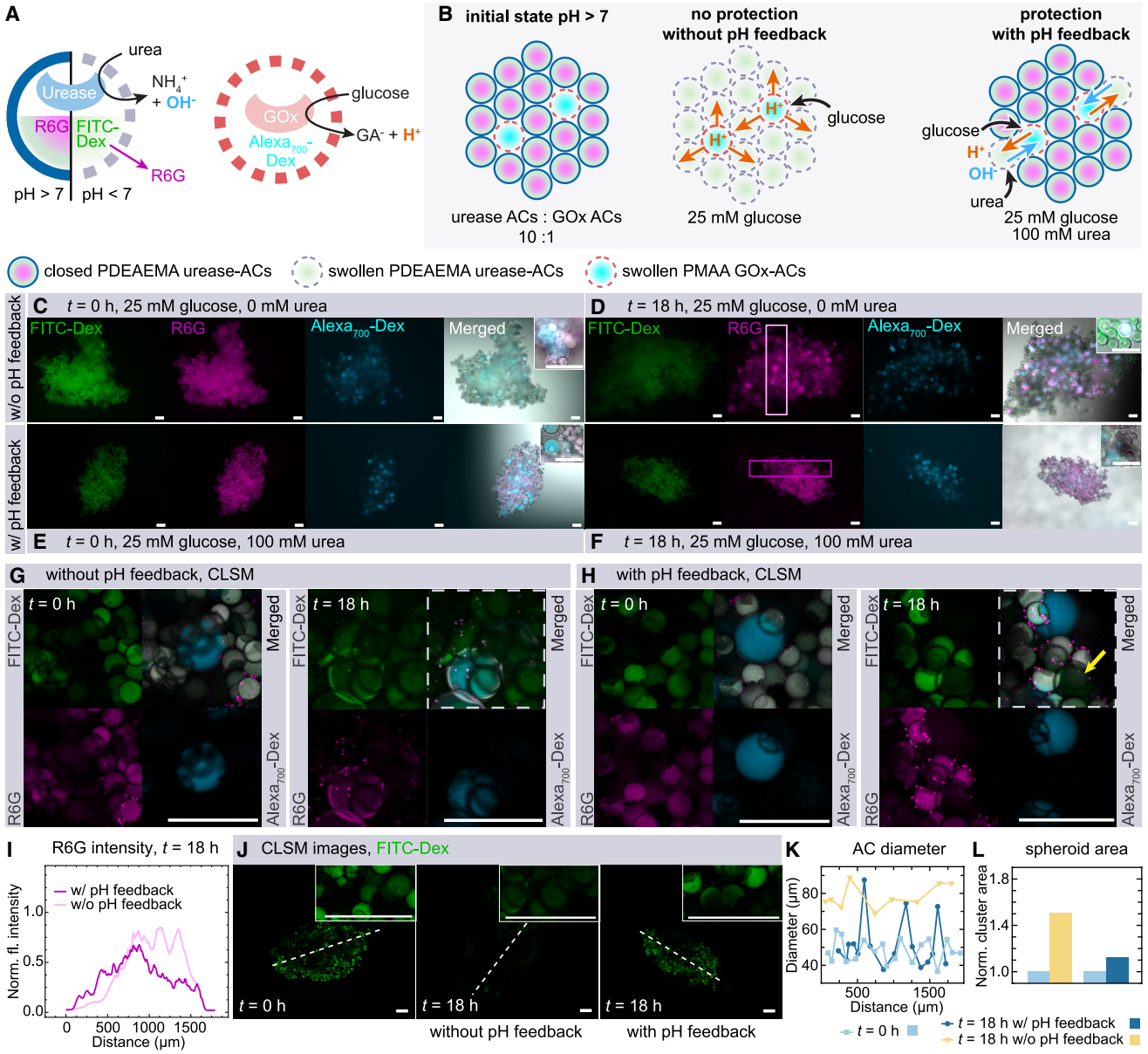

Figure 6. Urease-ACs within urease-AC/GOx-AC multi-AC spheroids at a 10:1 ratio enable a self-protection function through inter-AC communication

(A) Schematic of PMAA GOx-ACs (loaded with Alexa$_{700}$-Dex) as an internal acid source and PDEAEMA urease-ACs, which encapsulate R6G and FITC-Dex (500 kDa).

(B) Protection mechanism in multi-AC spheroids: initial state at pH > 7, no protection of R6G without pH feedback (w/o), and protection with pH feedback (w/, 100 mM urea).

(C–F) Fluorescence wide-field images of AC spheroids at t = 0 h and t = 18 h with and without pH feedback. Without pH feedback (25 mM glucose, 0 mM urea), urease-ACs swell and release R6G (C and D). With pH feedback (25 mM glucose, 100 mM urea), most urease-ACs remain closed and retain R6G (E and F). The AC spheroids in (C) and (D) represent the same spheroid, as do those in (E) and (F). Brightness and contrast of the Alexa$_{700}$-Dex channel in (F) was increased 2-fold. Scale bars: 200 μm.

(G and H) Close-up CLSM images of AC spheroids at t = 0 and 18 h without and with pH feedback, showing FITC-Dex and R6G distribution. The yellow arrow indicates a swollen urease-AC. Scale bars: 200 μm.

(I) Normalized fluorescence intensity of R6G at t = 18 h with and without pH feedback; measured in (D) and (F), as highlighted in rectangular boxes.

(J) CLSM images of FITC-Dex at t = 0 h and t = 18 h without and with pH feedback. Scale bars: 200 μm.

(K) Urease-AC diameter analysis over distance, showing swelling only in the outer regions with pH feedback. Diameters were calculated from CLSM images in (J) along the dashed lines.

(L) Comparison of normalized spheroid area increase at t = 0 h and t = 18 h without and with pH feedback. The area was measured from wide-field images in (C)–(F).

Materials availability

This study did not generate new unique reagents.

Data and code availability

All data supporting the conclusions of this study are available in the main text and supplemental information or from the lead contact upon reasonable request.

ACKNOWLEDGMENTS

We acknowledge discussions with K. Landfester (MPI for Polymer Research, Mainz) and R. von Klitzing (TU Darmstadt). We acknowledge the financial support of the DFG through the SFB 1066 project B14. A.W. acknowledges funding through a Max Planck Fellowship and a Gutenberg Research Fellowship underpinning his life-like materials program. M.M. acknowledges funding by the Marie Curie program with grant MSCA-2022-PF-01-01.

AUTHOR CONTRIBUTIONS

A.W. conceived the project. J.K. designed and performed the experiments and conducted the data analysis and visualization. J.K. and A.W. wrote the manuscript. C.-R.L. and E.A. supported the development and setup of the microfluidic production process. M.M. designed the microfluidics chip. All authors commented on the manuscript.

DECLARATION OF INTERESTS

The authors declare no competing interests.

SUPPLEMENTAL INFORMATION

Supplemental information can be found online at https://doi.org/10.1016/j.chempr.2024.102409.

Received: September 12, 2024
Revised: November 27, 2024
Accepted: December 30, 2024
Published: February 7, 2025

REFERENCES

1. Zinner, M., Lukonin, I., and Liberali, P. (2020). Design principles of tissue organisation: how single cells coordinate across scales. Curr. Opin. Cell Biol. *67*, 37–45. https://doi.org/10.1016/j.ceb.2020.07.004.
2. Hense, B.A., Kuttler, C., Müller, J., Rothballer, M., Hartmann, A., and Kreft, J.-U. (2007). Does efficiency sensing unify diffusion and quorum sensing? Nat. Rev. Microbiol. *5*, 230–239. https://doi.org/10.1038/nrmicro1600.
3. Buddingh', B.C., Elzinga, J., and Van Hest, J.C.M. (2020). Intercellular communication between artificial cells by allosteric amplification of a molecular signal. Nat. Commun. *11*, 1652. https://doi.org/10.1038/s41467-020-15482-8.
4. Van Veldhuisen, T.W., Verwiel, M.A.M., Novosedlik, S., Brunsveld, L., and Van Hest, J.C.M. (2024). Competitive protein recruitment in artificial cells. Commun. Chem. *7*, 148. https://doi.org/10.1038/s42004-024-01229-9.
5. Kurihara, K., Tamura, M., Shohda, K.I., Toyota, T., Suzuki, K., and Sugawara, T. (2011). Self-reproduction of supramolecular giant vesicles combined with the amplification of encapsulated DNA. Nat. Chem. *3*, 775–781. https://doi.org/10.1038/nchem.1127.
6. Adamala, K.P., Martin-Alarcon, D.A., Guthrie-Honea, K.R., and Boyden, E.S. (2017). Engineering genetic circuit interactions within and between synthetic minimal cells. Nat. Chem. *9*, 431–439. https://doi.org/10.1038/nchem.2644.
7. Weiss, M., Frohnmayer, J.P., Benk, L.T., Haller, B., Janiesch, J.-W., Heitkamp, T., Börsch, M., Lira, R.B., Dimova, R., Lipowsky, R., et al. (2018). Sequential bottom-up assembly of mechanically stabilized synthetic cells by microfluidics. Nat. Mater. *17*, 89–96. https://doi.org/10.1038/nmat5005.
8. Dubuc, E., Pieters, P.A., van der Linden, A.J., van Hest, J.C., Huck, W.T., and de Greef, T.F. (2019). Cell-free microcompartmentalised transcription–translation for the prototyping of synthetic communication networks. Curr. Opin. Biotechnol. *58*, 72–80. https://doi.org/10.1016/j.copbio.2018.10.006.
9. Cook, A.B., Novosedlik, S., and van Hest, J.C.M. (2023). Complex Coacervate Materials as Artificial Cells. Acc. Mater. Res. *4*, 287–298. https://doi.org/10.1021/accountsmr.2c00239.
10. Cao, S., Ivanov, T., Heuer, J., Ferguson, C.T.J., Landfester, K., and Caire da Silva, L. (2024). Dipeptide coacervates as artificial membraneless organelles for bioorthogonal catalysis. Nat. Commun. *15*, 39. https://doi.org/10.1038/s41467-023-44278-9.
11. Liu, W., Deng, J., Song, S., Sethi, S., and Walther, A. (2024). A facile DNA coacervate platform for engineering wetting, engulfment, fusion and transient behavior. Commun. Chem. *7*, 100. https://doi.org/10.1038/s42004-024-01185-4.
12. Samanta, A., Baranda Pellejero, L., Masukawa, M., and Walther, A. (2024). DNA-empowered synthetic cells as minimalistic life forms. Nat. Rev. Chem. *8*, 454–470. https://doi.org/10.1038/s41570-024-00606-1.
13. Maity, S., Ottelé, J., Santiago, G.M., Frederix, P.W.J.M., Kroon, P., Markovitch, O., Stuart, M.C.A., Marrink, S.J., Otto, S., and Roos, W.H. (2020). Caught in the Act: Mechanistic Insight into Supramolecular Polymerization-Driven Self-Replication from Real-Time Visualization. J. Am. Chem. Soc. *142*, 13709–13717. https://doi.org/10.1021/jacs.0c02635.
14. Zwicker, D., Seyboldt, R., Weber, C.A., Hyman, A.A., and Jülicher, F. (2017). Growth and division of active droplets provides a model for protocells. Nature Phys. *13*, 408–413. https://doi.org/10.1038/nphys3984.
15. Olivi, L., Berger, M., Creyghton, R.N.P., De Franceschi, N., Dekker, C., Mulder, B.M., Claassens, N.J., ten Wolde, P.R., and van der Oost, J. (2021). Towards a synthetic cell cycle. Nat. Commun. *12*, 4531. https://doi.org/10.1038/s41467-021-24772-8.
16. Tror, S., Jeon, S., Nguyen, H.T., Huh, E., and Shin, K. (2023). A Self-Regenerating Artificial Cell, that is One Step Closer to Living Cells: Challenges and Perspectives. Small Methods *7*, e2300182. https://doi.org/10.1002/smtd.202300182.
17. Tang, T.D., Cecchi, D., Fracasso, G., Accardi, D., Coutable-Pennarun, A., Mansy, S.S., Perriman, A.W., Anderson, J.L.R., and Mann, S. (2018). Gene-Mediated Chemical Communication in Synthetic Protocell Communities. ACS Synth. Biol. *7*, 339–346. https://doi.org/10.1021/acssynbio.7b00306.
18. Robinson, A.O., Venero, O.M., and Adamala, K.P. (2021). Toward synthetic life: Biomimetic synthetic cell communication. Curr. Opin. Chem. Biol. *64*, 165–173. https://doi.org/10.1016/j.cbpa.2021.08.008.
19. Niederholtmeyer, H., Chaggan, C., and Devaraj, N.K. (2018). Communication and quorum sensing in non-living mimics of eukaryotic cells. Nat. Commun. *9*, 5027. https://doi.org/10.1038/s41467-018-07473-7.
20. Joesaar, A., Yang, S., Bögels, B., Van Der Linden, A., Pieters, P., Kumar, B.V.V.S.P., Dalchau, N., Phillips, A., Mann, S., and De Greef, T.F.A. (2019). DNA-based communication in populations of synthetic protocells. Nat. Nanotechnol. *14*, 369–378. https://doi.org/10.1038/s41565-019-0399-9.
21. Belluati, A., Jimaja, S., Chadwick, R.J., Glynn, C., Chami, M., Happel, D., Guo, C., Kolmar, H., and Bruns, N. (2024). Artificial cell synthesis using biocatalytic polymerization-induced self-assembly. Nat. Chem. *16*, 564–574. https://doi.org/10.1038/s41557-023-01391-y.
22. Cheng, G., and Pérez-Mercader, J. (2019). Engineering Programmable Synthetic Vesicles with Permeability Regulated by a Single Molecular Bridge. Chem. Mater. *31*, 5691–5698. https://doi.org/10.1021/acs.chemmater.9b01635.
23. Cheng, G., Hao, S.-J., Wan, Y., Shan, D.-Y., Yang, J., and Zheng, S.-Y. (2017). Self-Assembly of Smart Multifunctional Hybrid Compartments

with Programmable Bioactivity. Chem. Mater. *29*, 2081–2089. https://doi.org/10.1021/acs.chemmater.6b04326.

24. Pearce, S., and Perez-Mercader, J. (2021). Chemoadaptive Polymeric Assemblies by Integrated Chemical Feedback in Self-Assembled Synthetic Protocells. ACS Cent. Sci. *7*, 1543–1550. https://doi.org/10.1021/acscentsci.1c00681.
25. Qi, C., Ma, X., Zhong, J., Fang, J., Huang, Y., Deng, X., Kong, T., and Liu, Z. (2023). Facile and Programmable Capillary-Induced Assembly of Prototissues via Hanging Drop Arrays. ACS Nano *17*, 16787–16797. https://doi.org/10.1021/acsnano.3c03516.
26. Casas-Ferrer, L., Brisson, A., Massiera, G., and Casanellas, L. (2021). Design of vesicle prototissues as a model for cellular tissues. Soft Matter *17*, 5061–5072. https://doi.org/10.1039/D1SM00336D.
27. Samanta, A., Hörner, M., Liu, W., Weber, W., and Walther, A. (2022). Signal-processing and adaptive prototissue formation in metabolic DNA protocells. Nat. Commun. *13*, 3968. https://doi.org/10.1038/s41467-022-31632-6.
28. Arulkumaran, N., Singer, M., Howorka, S., and Burns, J.R. (2023). Creating complex protocells and prototissues using simple DNA building blocks. Nat. Commun. *14*, 1314. https://doi.org/10.1038/s41467-023-36875-5.
29. Liu, S., Zhang, Y., He, X., Li, M., Huang, J., Yang, X., Wang, K., Mann, S., and Liu, J. (2022). Signal processing and generation of bioactive nitric oxide in a model prototissue. Nat. Commun. *13*, 5254. https://doi.org/10.1038/s41467-022-32941-6.
30. Ranganath, V.A., and Maity, I. (2024). Artificial Homeostasis Systems Based on Feedback Reaction Networks: Design Principles and Future Promises. Angew. Chem. Int. Ed. Engl. *63*, e202318134. https://doi.org/10.1002/anie.202318134.
31. Zhang, Q., Jian, L., Yao, D., Rao, B., Xia, Y., Hu, K., Li, S., Shen, Y., Cao, M., Qin, A., et al. (2023). The structural basis of the pH-homeostasis mediated by the Cl−/HCO3− exchanger, AE2. Nat. Commun. *14*, 1812. https://doi.org/10.1038/s41467-023-37557-y.
32. Sharma, C., Maity, I., and Walther, A. (2023). pH-feedback systems to program autonomous self-assembly and material lifecycles. Chem. Commun. (Camb) *59*, 1125–1144. https://doi.org/10.1039/D2CC06402B.
33. Krajewska, B. (2009). Ureases I. Functional, catalytic and kinetic properties: A review. Journal of Molecular Catalysis B: Enzymatic *59*, 9–21. https://doi.org/10.1016/j.molcatb.2009.01.003.
34. Heuser, T., Weyandt, E., and Walther, A. (2015). Biocatalytic Feedback-Driven Temporal Programming of Self-Regulating Peptide Hydrogels. Angew. Chem. Int. Ed. Engl. *54*, 13258–13262. https://doi.org/10.1002/anie.201505013.
35. Heuser, T., Merindol, R., Loescher, S., Klaus, A., and Walther, A. (2017). Photonic Devices Out of Equilibrium: Transient Memory, Signal Propagation, and Sensing. Adv. Mater. *29*, 1606842. https://doi.org/10.1002/adma.201606842.
36. Heinen, L., Heuser, T., Steinschulte, A., and Walther, A. (2017). Antagonistic Enzymes in a Biocatalytic pH Feedback System Program Autonomous DNA Hydrogel Life Cycles. Nano Lett. *17*, 4989–4995. https://doi.org/10.1021/acs.nanolett.7b02165.
37. Miele, Y., Jones, S.J., Rossi, F., Beales, P.A., and Taylor, A.F. (2022). Collective Behavior of Urease pH Clocks in Nano- and Microvesicles Controlled by Fast Ammonia Transport. J. Phys. Chem. Lett. *13*, 1979–1984. https://doi.org/10.1021/acs.jpclett.2c00069.
38. Wang, D., Moreno, S., Boye, S., Voit, B., and Appelhans, D. (2021). Detection of subtle extracellular glucose changes by artificial organelles in protocells. Chem. Commun. (Camb) *57*, 8019–8022. https://doi.org/10.1039/D1CC03422G.
39. Wen, P., Wang, X., Moreno, S., Boye, S., Voigt, D., Voit, B., Huang, X., and Appelhans, D. (2021). Construction of Eukaryotic Cell Biomimetics: Hierarchical Polymersomes-in-Proteinosome Multicompartment with Enzymatic Reactions Modulated Protein Transportation. Small *17*, e2005749. https://doi.org/10.1002/smll.202005749.
40. Zhang, K., Moreno, S., Wang, X., Zhou, Y., Boye, S., Voigt, D., Voit, B., and Appelhans, D. (2023). Biomimetic Cell Structures: Probing Induced pH-Feedback Loops and pH Self-Monitoring in Cytosol Using Binary Enzyme-Loaded Polymersomes in Proteinosome. Biomacromolecules *24*, 2489–2500. https://doi.org/10.1021/acs.biomac.3c00010.
41. Wang, X., Moreno, S., Boye, S., Wen, P., Zhang, K., Formanek, P., Lederer, A., Voit, B., and Appelhans, D. (2021). Feedback-Induced and Oscillating pH Regulation of a Binary Enzyme–Polymersomes System. Chem. Mater. *33*, 6692–6700. https://doi.org/10.1021/acs.chemmater.1c00897.
42. Maity, I., Sharma, C., Lossada, F., and Walther, A. (2021). Feedback and Communication in Active Hydrogel Spheres with pH Fronts: Facile Approaches to Grow Soft Hydrogel Structures. Angew. Chem. Int. Ed. Engl. *60*, 22537–22546. https://doi.org/10.1002/anie.202109735.
43. Che, H., Cao, S., and van Hest, J.C.M. (2018). Feedback-Induced Temporal Control of "Breathing" Polymersomes To Create Self-Adaptive Nanoreactors. J. Am. Chem. Soc. *140*, 5356–5359. https://doi.org/10.1021/jacs.8b02387.
44. Van Den Akker, W.P., Wu, H., Welzen, P.L.W., Friedrich, H., Abdelmohsen, L.K.E.A., Van Benthem, R.A.T.M., Voets, I.K., and Van Hest, J.C.M. (2023). Nonlinear Transient Permeability in pH-Responsive Bicontinuous Nanospheres. J. Am. Chem. Soc. *145*, 8600–8608. https://doi.org/10.1021/jacs.3c01203.
45. van den Akker, W.P., van Benthem, R.A.T.M., Voets, I.K., and van Hest, J.C.M. (2024). Dampened Transient Actuation of Hydrogels Autonomously Controlled by pH-Responsive Bicontinuous Nanospheres. ACS Appl. Mater. Interfaces *16*, 19642–19650. https://doi.org/10.1021/acsami.4c02643.
46. Rifaie-Graham, O., Yeow, J., Najer, A., Wang, R., Sun, R., Zhou, K., Dell, T.N., Adrianus, C., Thanapongpibul, C., Chami, M., et al. (2023). Photoswitchable gating of non-equilibrium enzymatic feedback in chemically communicating polymersome nanoreactors. Nat. Chem. *15*, 110–118. https://doi.org/10.1038/s41557-022-01062-4.
47. Arriaga, L.R., Amstad, E., and Weitz, D.A. (2015). Scalable single-step microfluidic production of single-core double emulsions with ultra-thin shells. Lab Chip *15*, 3335–3340. https://doi.org/10.1039/C5LC00631G.
48. Werner, J.G., Nawar, S., Solovev, A.A., and Weitz, D.A. (2018). Hydrogel Microcapsules with Dynamic pH-Responsive Properties from Methacrylic Anhydride. Macromolecules *51*, 5798–5805. https://doi.org/10.1021/acs.macromol.8b00843.
49. Fan, X., and Walther, A. (2021). pH Feedback Lifecycles Programmed by Enzymatic Logic Gates Using Common Foods as Fuels. Angew. Chem. Int. Ed. Engl. *60*, 11398–11405. https://doi.org/10.1002/anie.202017003.
50. Heuser, T., Steppert, A.-K., Lopez, C.M., Zhu, B., and Walther, A. (2015). Generic Concept to Program the Time Domain of Self-Assemblies with a Self-Regulation Mechanism. Nano Lett. *15*, 2213–2219. https://doi.org/10.1021/nl5039506.
51. Bohn, T., Rapp, S., Luther, N., Klein, M., Bruehl, T.-J., Kojima, N., Aranda Lopez, P., Hahlbrock, J., Muth, S., Endo, S., et al. (2018). Tumor immunoevasion via acidosis-dependent induction of regulatory tumor-associated macrophages. Nat. Immunol. *19*, 1319–1329. https://doi.org/10.1038/s41590-018-0226-8.